Volume 7 | Number 5 | May 2019 | Pages 1731–2202

# Biomaterials Science

rsc.li/biomaterials-science

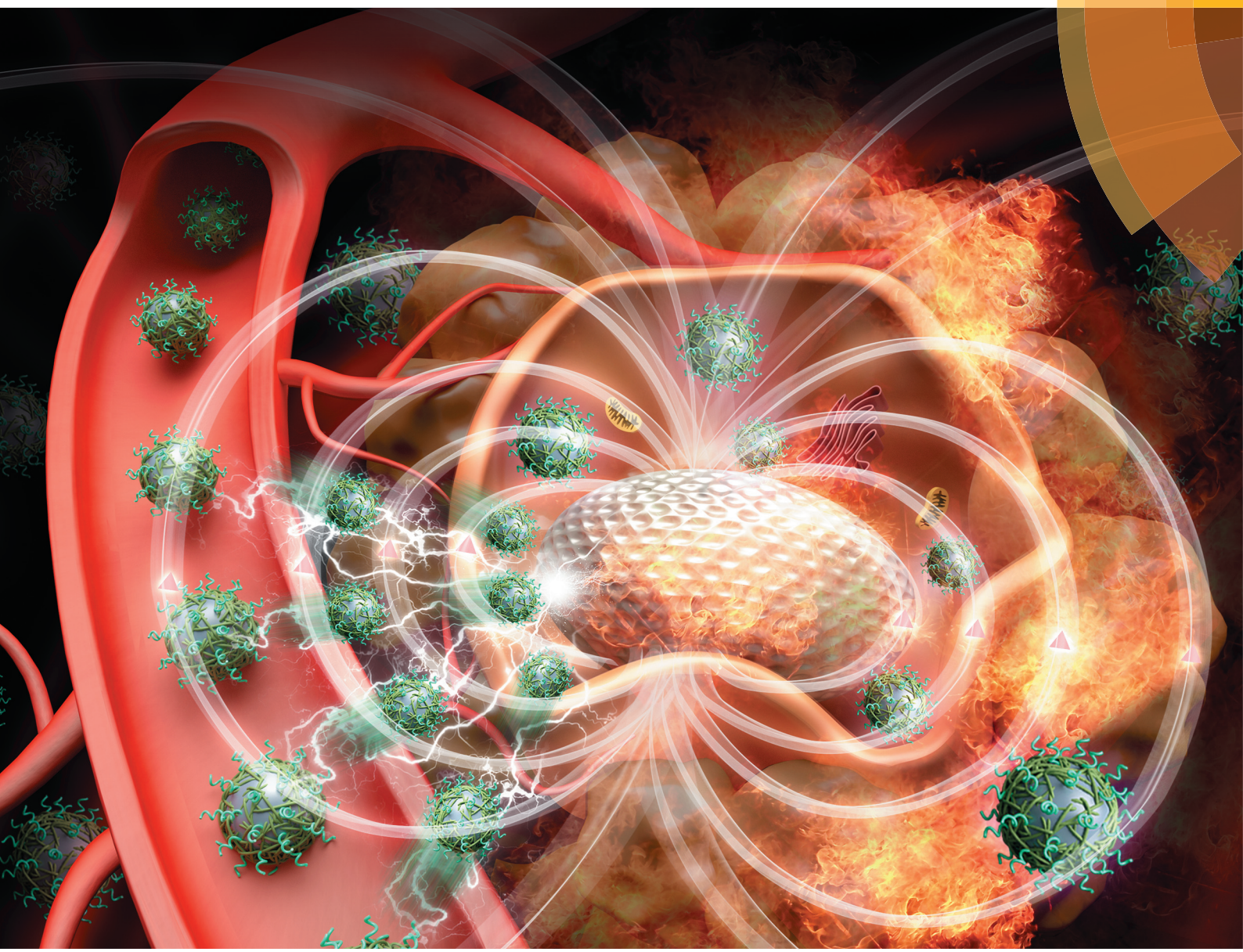

ISSN 2047-4849

ROYAL SOCIETY OF CHEMISTRY | Celebrating IYPT 2019

COMMUNICATION

Guoqing Zuo, Yu Chen, Yuanyi Zheng *et al.*

An artificially engineered "tumor bio-magnet" for collecting blood-circulating nanoparticles and magnetic hyperthermia

ESB European Society for Biomaterials

Biomaterials Science

COMMUNICATION

View Article Online
View Journal | View Issue



Cite this: *Biomater. Sci.*, 2019, **7**, 1815

Received 20th December 2018,
Accepted 7th March 2019

DOI: 10.1039/c8bm01658e

rsc.li/biomaterials-science



# An artificially engineered "tumor bio-magnet" for collecting blood-circulating nanoparticles and magnetic hyperthermia†

Bing Liang, ‡[a] Kexiao Yu, ‡[a] Yi Ling,‡[a] Micheal Kolios, [b] Agata Exner, [c] Zhigang Wang,[a] Bing Hu,[d] Guoqing Zuo,*[a,e] Yu Chen *[f] and Yuanyi Zheng *[a,d]

**It is a great challenge to directly endow a tumor with specific functions for theranostic treatment. In this study, we report on a novel approach to transform a tumor into a "bio-magnet", to be magnetized on demand, in order to create an intrinsic tumor magnetic field that would collect magnetic nanoparticles (MNPs) circulating in the blood and achieve simultaneous magnetic hyperthermia. This was achieved by the localized intratumoral injection of liquid $Nd_2Fe_{14}B/Fe_3O_4$-PLGA, followed by solvent exchange that induces a liquid-to-solid transformation. After the magnetism charging process, the solid $Nd_2Fe_{14}B/Fe_3O_4$-PLGA implant was endowed with permanent magnetic properties and *in situ* created the magnetic field within the tumor tissue, making the tumor a "bio-magnet". After the creation of the bio-magnet, intravenously injected MNPs accumulated into the tumor tissue due to the tumor magnetic field. Importantly, both the *in vitro* and *ex vivo* results demonstrated the high efficiency of the implanted bio-magnet for magnetic hyperthermia. This new approach achieves magnetic targeting by creating a tumor "bio-magnet", which generates a strong magnetic field within the tumor, paving a new way for the development of an efficient targeting strategy for tumor therapy.**

## Introduction

Cancer is now one of the biggest challenges threatening human health.[1,2] Although traditional therapeutic modalities have found their roles in cancer therapy (*e.g.*, chemotherapy, surgery, radiotherapy),[3–5] patient compliance is relatively low because of severe side effects.[6] The development of new therapeutic modalities that minimize normal tissue damage and target tumor tissue has long been a goal in cancer treatment.[7,8] For instance, targeted chemotherapy can realize high tumor accumulation and therefore enhanced therapeutic efficiency.[9–11] However, targeted drug delivery still has shortcomings that need to be solved.[12,13] On one hand, the targeting efficiency is unfortunately still too low to achieve the desirable chemotherapeutic outcome.[14,15] On the other hand, the targeting is time-consuming, tedious and expensive, creating significant barriers to the clinical translation of these targeting strategies.[16–18] The emergence of nanotechnology and nanomedicine employing various nanoparticles as the nano-based drug delivery system (DDS) can enhance the drug-delivery efficiency *via* enhanced permeability and retention (EPR) effect-based passively-targeted accumulation.[19–23] However, it has been shown that relying on passive accumulation is not efficient since the densely packed extra-cellular matrix (ECM) of early-stage tumors appears to sterically restrict nanoparticle accumulation based on particle diameter.[24] Magnetic nanoparticles (MNPs) have been explored as the promising DDS for theranostic applications, including magnetic hyperthermia,[25–27] drug delivery,[28–30] and diagnostic imaging.[31,32] Importantly, these MNPs can be manipulated by an external magnetic field to achieve active targeting by magnetic field-targeted transportation.[33–35]

Conjugation of MNPs with drugs in combination with an external magnetic field to target the MNPs to the target tissues

[a]*Institute of Ultrasound Imaging of Chongqing Medical University, Second Affiliated Hospital of Chongqing Medical University, 76 Linjiang Road, Yuzhong Distinct, Chongqing, 400010, P. R. China. E-mail: cqzgqly@163.com, zhengyuanyi@163.com*
[b]*Department of Physics, Ryerson University, Toronto, 350 Victoria Street Toronto, Ontario M5B 2 K3, Ontario, Canada*
[c]*Radiology department of University Hospital, Case Western Reserve University, 10900 Euclid Ave, Cleveland, OH, 44106, USA*
[d]*Shanghai Jiao Tong University Affiliated Sixth People's Hospital, 600 Yishan Road, Xuhui Distinct, Shanghai, 200233, P. R. China*
[e]*Chongqing Hospital of Traditional Chinese Medicine, 6 Panxi Road, JiangBei Distinct, Chongqing, 400021, P. R. China*
[f]*State Key Lab of High Performance Ceramics and Superfine Microstructure, Shanghai Institute of Ceramics, Chinese Academy of Sciences, Shanghai, 200050, P. R. China. E-mail: chenyu@mail.sic.ac.cn*

†Electronic supplementary information (ESI) available: Experimental section, schematic of the *in vivo* application of artificial bio-magnet in collecting MNPs, the magnetic hysteresis loop of the initial $Nd_2Fe_{14}B$ and $Fe_3O_4$ particles ultrasound imaging of the phase-transformation procedure, SEM and EDS results of MNPs and $Nd_2Fe_{14}B/Fe_3O_4$-PLGA; video of the preparation of $Nd_2Fe_{14}B/Fe_3O_4$-PLGA, liquid–solid transformation, and magnetism test results of 60 μL, 80 μL, 100 μL bio-magents. See DOI: 10.1039/c8bm01658e

‡These authors are co-first authors who contributed equally to this study.

(so-called "magnetic drug targeting", MDT) has emerged as a promising strategy for targeted drug delivery.[36,37] The MNP-based therapy has been suggested as a non-invasive and relatively non-toxic protocol for cancer treatment.[33] However, there are still some critical issues to be solved for efficient MNP targeted drug delivery. First, magnetic targeting typically requires an external magnetic field, which is expensive, technologically complex and for which the field is difficult to focus.[38] Second, relying on the passive accumulation of MNPs is not optimal due to the lack of control or the particle intratumoral distribution and normal tissue cytotoxicity.[39] Third, current approaches using MNPs still suffer from low-targeting efficiency under external magnetic fields because of the limitations of the magnetic field strengths and conformity that can be achieved *in vivo*.[40,41] Therefore, it is highly desirable to develop new magnetic-targeting strategies for efficient cancer therapy.

To overcome the above limitations, our proposed new approach relies on an injectable and chargeable bio-magnet that is based on a smart phase-transition organic/inorganic hybrid implant, which can be injected in liquid form in tissue before solidifying. Upon the magnetization of the bio-magnet, MNPs in the circulation would accumulate at the location of the intratumoral injection to facilitate magnetic-hyperthermia of the tumor. This unique bio-magnet could be directly injected into the center of the tumor in a minimally invasive manner under real-time ultrasound-imaging guidance based on its high fluidity and syringeability. It is noted that neodymium iron boron ($Nd_2Fe_{14}B$)[42,43] and intratumoral injections have been extensively used clinically (*e.g.*, IntraDose, Cisplatin/Epinephrine Injectable Gel, an FDA approved drug) and in basic research, which are suitable for the chemotherapy of tumors at the last stage or tumors without abundant blood supply. After contacting water, the liquid bio-magnet transforms into a solid form based on a specific solvent-exchange process. The solidification of the gel firmly confines the implant within the tumor to avoid material/drug leakage and minimize the exposure to the normal tissue. An additional magnetizing process on the post-formed solid implant endowed the bio-magnet with strong magnetic properties to create an intrinsic magnetic field within the tumor for absorbing the circulating MNPs. The bio-magnet within the tumor could also respond to external alternating current (a. c.) magnetic fields to achieve localized magnetic hyperthermia. It is highly expected that the dual functions of the implanted bio-magnet within the tumor (*i.e.* aiding in the targeting of MNPs and providing material for magnetic hyperthermia) provide a new efficient strategy for cancer therapy based on the delivery of magnetic biomaterials.

## Results and discussion

A unique artificial bio-magnet for implantation within the tumor tissue has been developed to create an intrinsically magnetic field within a tumor for realizing concurrent targeting of the blood-circulating MNPs and localized magnetic hyperthermia. As shown in Fig. 1a, hydrophobic organic polylactic-*co*-glycolic acid (PLGA) molecule is capable of dissolving into *N*-methyl pyrrolidone (NMP) solvent to form a homogenous solution.[44] Although NMP has low toxicity, as a constituent in medical devices, it has been widely used and approved by the Food and Drug Administration.[45] Concise International Chemical Assessment Document (No. 35, 2006) from World Health Organization was reported that NMP repeated daily doses of 450 mg per kg body weight administered to the skin could cause painful haemorrhage and eschar formation in rabbits. However, in our study, the locally injected NMP was only 75 μL (net content 0.005 mg $kg^{-1}$) in each mouse, which is far below the toxic dose. As Video S1† shows, $Nd_2Fe_{14}B$ and $Fe_3O_4$ particles before being charged could easily be dispersed into the above solution by mechanical vibration (Fig. 1a Step 1),[44,46] the magnetic hysteresis loop of the initial $Nd_2Fe_{14}B$ and $Fe_3O_4$ particles is shown in Fig. S2 and S3,† respectively. After injecting into the aqueous solution, the NMP solvent quickly exchanges with surrounding water, causing the precipitation of hydrophobic PLGA containing $Nd_2Fe_{14}B$ and $Fe_3O_4$ particles and forming a solid implant (Step 2). After establishing a tumor xenograft (Fig. S1a and e†), the as-formed $Nd_2Fe_{14}B$/$Fe_3O_4$-PLGA bio-injection could easily be injected into the center of the tumor tissue (Fig. S1b and f†). Because of the aqueous tumor microenvironment, the solvent-exchanging process occured, leaving the solid implant firmly confined within the tumor tissue. The following magnetism-charging process directly transforms the magnetic implant into a bio-magnet (Fig. S1c and S1g†), which is capable of collecting the blood-circulating MNPs for intrinsic magnetic field-guided tumor targeting ((Fig. S1d and h†) and magnetic hyperthermia (Fig. 1b).

To show the high syringeability and fluidity of the as-prepared $Nd_2Fe_{14}B/Fe_3O_4$-PLGA bio-injection facilitating minimally invasive localized injection, $Nd_2Fe_{14}B/Fe_3O_4$-PLGA was loaded into a standard syringe (Fig. 2a). It has been found that the $Nd_2Fe_{14}B/Fe_3O_4$-PLGA bio-injection could easily and freely pass through the syringe based on the low viscosity of the NMP solvent (Fig. 2b and Video S2†). The phase transformation took place immediately after contacting with water (Fig. 2c–e and Video S2†) because of the fast solvent exchange process between NMP and water. Such a quick phase-changing process was further monitored both *in vitro* (Fig. 2f–i and Fig. S4†) and *in vivo* (Fig. 2j and k) by ultrasound imaging. An obvious contrast enhancement of ultrasound imaging was observed after liquid-to-solid phase transformation (Fig. 2f–i). Importantly, the post-formed solid implant was confined in the interior of the tumor tissue, as confirmed by ultrasound imaging (Fig. 2k), facilitating the subsequent magnetism-charging process, MNP collection and magnetic hyperthermia. An SEM image shows the rough surface of the post-formed solid $Nd_2Fe_{14}B/Fe_3O_4$-PLGA implant (Fig. 2l). The presence of $Nd_2Fe_{14}B$ and $Fe_3O_4$ was further demonstrated by EDS and corresponding element mapping (Fig. S5†). The uniform distribution of the elements Nb, Fe and B indicates the homogeneous dispersity of $Nd_2Fe_{14}B$ and $Fe_3O_4$ within the matrix of the post-formed composite implant (Fig. 2m–q) after the liquid–solid phase transformation.

 

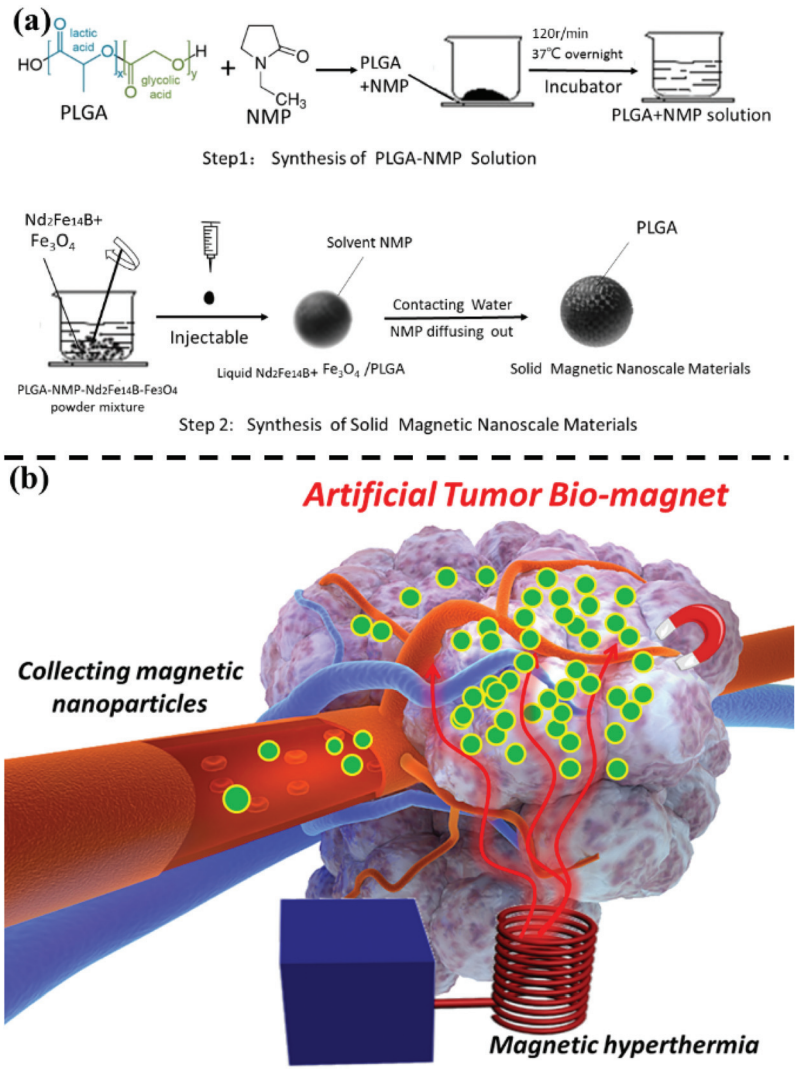


**Fig. 1** Schematic of the *in vitro* and *in vivo* application of artificial bio-magnet and its applications in collecting MNPs from the blood-vessel circulation. (a) The preparation of the $Nd_2Fe_{14}B/Fe_3O_4$-PLGA bio-injection and its further transformation into the bio-magnet. (b) The scheme of the artificial tumor bio-magnet with dual functions, including collecting the blood-circulating MNPs and magnetic hyperthermia.

It has been preliminarily demonstrated that external magnetic targeting can enhance the accumulation of MNPs in a tumor.[31,47] Herein, it was expected that the magnetic targeting efficiency could be significantly enhanced if the tumor could intrinsically become the magnet to collect the circulating MNPs. To achieve this, a novel magnetism-charging technique was developed to directly transform the implanted $Nd_2Fe_{14}B/Fe_3O_4$-PLGA magnetic composites into a bio-magnet for the generation of a unique artificial tumor bio-magnet with intrinsic magnetic field for collecting the circulating MNPs.

The $Nd_2Fe_{14}B$ component of the solid $Nd_2Fe_{14}B/Fe_3O_4$-PLGA implant could be directly transformed into a permanent magnet after magnetization. It has been demonstrated that the efficient magnetic targeting is based on two primary factors: magnetic field strength and the properties of the magnetic-responsive blood-circulating MNPs.[48,49] Its morphology and elementary composition are shown in Fig. S6.† As a preliminary experiment, MNPs were directly injected into a simulated blood vessel, followed by the introduction of the artificial bio-magnet into the center (Fig. 3a–f). The fluorescent MNPs were quickly immobilized by the magnetic field originating from the bio-magnet, possibly caused by the aggregation-induced fluorescent quenching[50] (Fig. 3e and f). Importantly, the $Nd_2Fe_{14}B/Fe_3O_4$-PLGA bio-magnet exhibited the expected magnetic field lines (Fig. 3g) and the bio-magnet is able to collect the surrounding MNPs easily (Fig. 3h and i), indicating that it could also potentially attract circulating MNPs in blood vessels. The magnetism of the as-formed bio-magnet was systematically characterized using bio-magnets with different $Nd_2Fe_{14}B$ percentages and adopted volumes (Fig. 3j). Furthermore, after adopting higher quality $Nd_2Fe_{14}B$, the magnetism could be further improved. For example, the magnetism for 100 μL of 65% $Nd_2Fe_{14}B$-bio-magnet was increased to over 1000 Gs (Videos S3, S4 and S5†). The increase in the

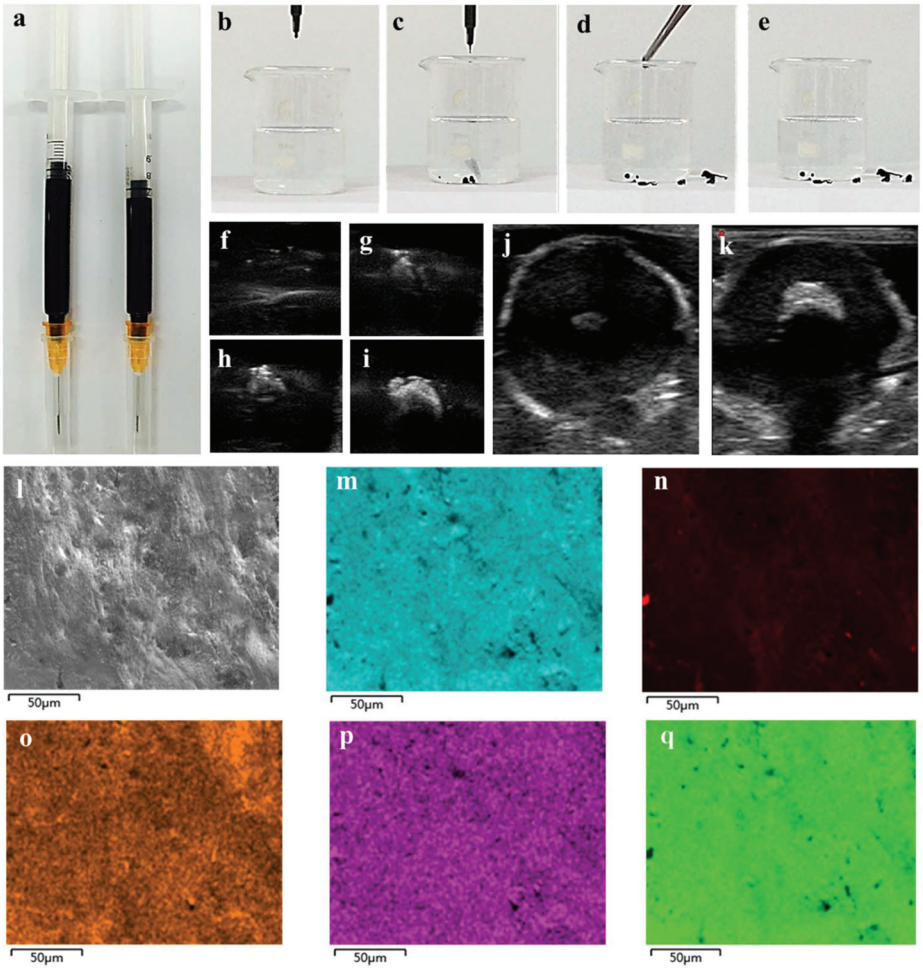


**Fig. 2** Characterization of the solid bio-magnet. (a) Digital photos of the injectable $Nd_2Fe_{14}B/Fe_3O_4$-PLGA though the standard 1 ml syringe and (b–e) the corresponding phase-change process after contacting the water. Real-time monitoring of the liquid-to-solid phase transition by ultrasound imaging both (f–i) *in vitro* and (j: before injection; k: after injection) *in vivo* in tumor xenograft. (l) SEM image of post-formed $Nd_2Fe_{14}B/Fe_3O_4$-PLGA solid implant and corresponding element mappings (m: Fe, n: C, o: Nd, p: B and q: O).

$Nd_2Fe_{14}B$ content within the composite implant could enhance the bio-magnet field strength, which is believed to be strong enough for the *in vivo* absorption of the circulating MNPs within the blood vessel. The magnetic hysteresis loop of the 65% $Nd_2Fe_{14}B$-bio-magnet clearly shows that this bio-magnet had a saturation magnetization as high as 126.0 emu $g^{-1}$ (Fig. 3k).

In order to evaluate magnetism of the bio-magnet *in vivo*, we further chose fluorescent MNPs to show the *in vivo* magnetic-targeting performance assisted by the implanted bio-magnet in nude mice bearing SMMC-7721 human HCC xenograft. As shown in Fig. 4a–d, the intravenously administered fluorescent MNPs gradually accumulated into the tumor with the extension of the circulating duration, demonstrating the high collecting performance of the implanted bio-magnet. Comparatively, the control group (A), the PLGA group (B), and $Nd_2Fe_{14}B/Fe_3O_4$-PLGA without charging group (C) have no obvious MNP accumulation. The efficient magnetic-targeting of the implanted bio-magnet was further demonstrated by the quantitative determination of the tumor fluorescent intensity, which originated from the accumulated MNPs (Fig. 4j). The fluorescent intensity increased significantly ($(11.36 \pm 2.46) \times 10^8$) compared to the group without magnetic targeting ($(1.94 \pm 0.86) \times 10^8$) after 48 h. In addition, the prussian-blue staining of the tumor before (Fig. 4e) and after the intravenous administration of MNPs (24 h, 48 h and 72 h) shows the substantially enhanced prussian blue-stained tumor tissues could be identified because of the high accumulation of MNPs into the tumor (Fig. 4f–h), further demonstrating the high magnetic-collecting efficacy of MNPs for tumor targeting. The elaborately introduced artificial bio-magnet formed a permanent magnetic field intrinsically within the tumor tissue (Fig. 4i). Therefore, the blood-circulating MNPs in the tumor vasculature could be targeted to the tumor, causing the high accumulation of the fluorescent MNPs. This result is very intriguing as it can effectively realize the nanoparticle targeting simply by creating the elaborately designed magnetic field within the tumor based on the artificial tumor bio-magnet. The contradictory findings for the *in vivo* and *in vitro* fluo-

 

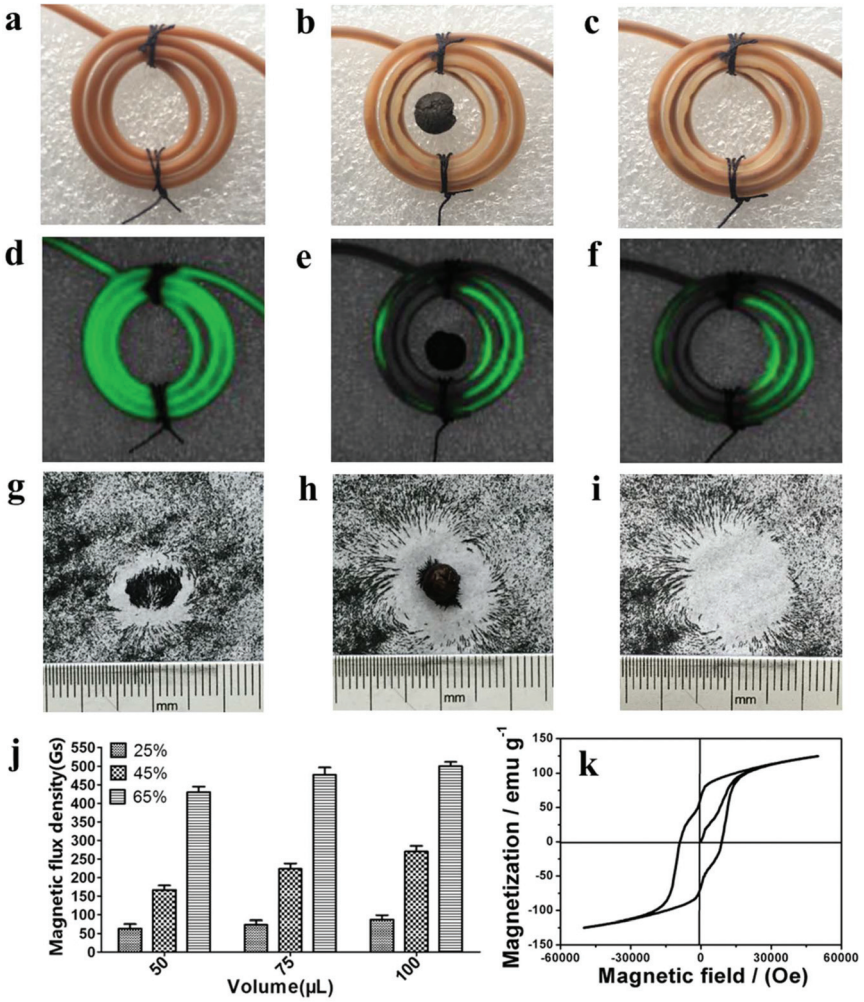


**Fig. 3** *In vitro* magnetic property and magnetic-guidance performance of the solid bio-magnet. (a–c) Photographs and (d–f) the corresponding fluorescent images of simulated blood vessels containing fluorescent superparamagnetic nanoparticles before and after the introduction of a magnetic field from the solid bio-magnet (a, d: before magnetic guidance; b, e: after magnetic guidance; c, f: bio-magnet removal after magnetic guidance). (g–i) Magnetic-induction line and magnetic absorption range of a 65% $Nd_2Fe_{14}B$-bio-magnet (75 μL liquid-transformed solid implant followed by magnetism charging). (j) The histogram of the magnetic-flux density of 75 μL bio-magnet with different $Nd_2Fe_{14}B$ contents and volume. (k) Magnetic hysteresis loop of 65% $Nd_2Fe_{14}B$-bio-magnet.

rescence phenomenon have been confirmed in this study, which is very interesting, while the detailed mechanism is unknown, which needs to be further studied in future. It was reported that the *in vitro* magnetic quenching of fluorescence might be caused by a large amount of fluorescent superparamagnetic nanoparticles at a high density.[50] The mechanism of magnetic quenching is only explored in the gas phase. The reason of magnetic quenching is the excited state particle interactions.[51] The possible reason for no quenching phenomenon *in vivo*, we think, might be the following: *in vivo* study, the concentrated particles dispersed inside the tissue, the tissue might have effect on the fluorescence, while it needs to be disclosed in future how the tissue affects the fluorescence.

In addition to the intriguing property of the implanted bio-magnet for collecting the circulating MNPs, the approach can also be used to enhance magnetic hyperthermia due to the bio-magnet's magnetic properties. It has been found that the presence of a bio-magnet could effectively and quickly increase the temperature of the surrounding microenvironment (Fig. 5a–c). Pure PLGA without magnetic materials showed no significant temperature variations (32.3 ± 0.5 °C and 35 ± 1.3 °C). The 65% $Nd_2Fe_{14}B$-bio-magnet achieved the highest temperature by the exposure to ac magnetic field only for three minutes. The temperatures of 50 μL, 75 μL, and 100 μL of 65% $Nd_2Fe_{14}B$-bio-magnet after three-minutes exposure were determined to be 87.3 ± 1.8 °C, 104.4 ± 2.2 °C and 125.9 ± 7.1 °C, respectively, based on the near infrared thermal measurements (Fig. 5c). It is noted that this hyperthermia temperature could easily reach over 45 °C, which is over the temperature threshold for potential tissue ablation and the temperature of the bio-magnet is controllable. The increase in the $Nd_2Fe_{14}B$

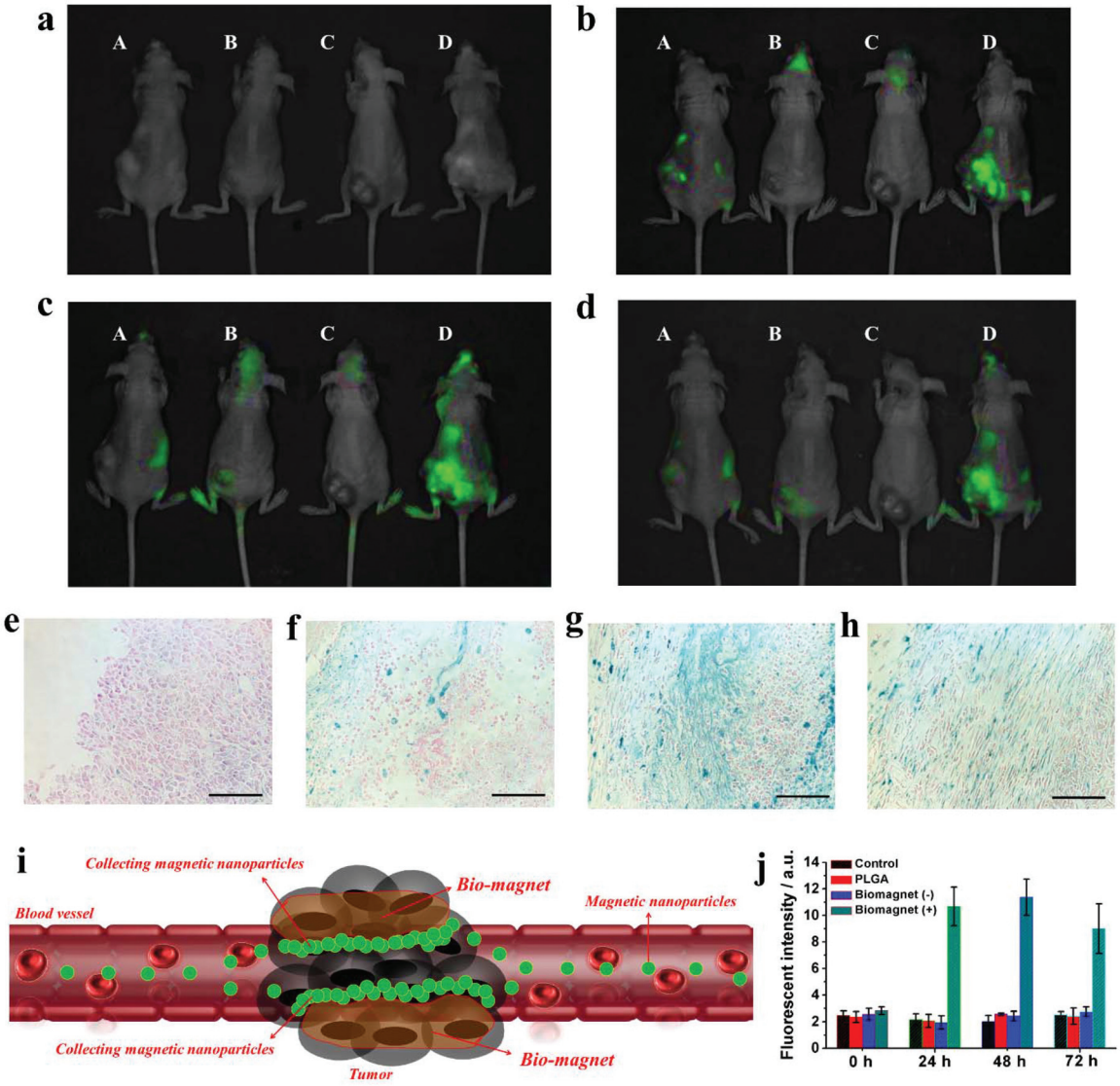


**Fig. 4** *In vivo* targeting of the circulating MNPs by the charged bio-magnet. *In vivo* fluorescent imaging of the tumor-bearing mice after the implantation with (B) 75 μL PLGA, (C) 75 μL 65% $Nd_2Fe_{14}B/Fe_3O_4$-PLGA without charging, (D) 75 μL $Nd_2Fe_{14}B$-bio-magnet followed by intravenous the administration of MNPs for (b) 24 h, (c) 48 h and (d) 72 h (a: before administration, A: control blank). Prussian-blue staining of the tumors (e) before injecting MNPs and after the intravenous injection for (f) 24 h, (g) 48 h and (h) 72 h (scar bar: 200 μm). (j) The fluorescent intensities corresponding to images a–d. (i) Schematic of the introduction of the artificial bio-magnet within the tumor tissue for collecting blood-circulating MNPs.

content could also enhance the hyperthermia ablation outcome of the bio-magnet (Fig. 5b).

To further demonstrate the therapeutic efficiency of the bio-magnet for magnetic hyperthermia, bovine liver was initially chosen for an *ex vivo* evaluation. The temperature of the bovine liver after implanting 75 μL 65%-bio-magnet exhibited a quick increase after exposure to ac magnetic field (Fig. 5e). The bovine liver without the bio-magnet implant (Fig. 5d), however, showed no significant temperature increase after the magnetic-field exposure (Fig. 5f). The high temperatures caused significant tissue ablation. The ablation efficiency strongly depends on the exposure duration and the adopted content of the bio-magnet (Fig. 5g). Therefore, it is also expected that the implantation of the bio-magnet is potentially capable of hyperthermia ablation of the tumor based on its high magnetic-heat conversion efficiency, or in assisting the magnetic-targeting chemotherapy based on the bio-magnet magnetic field-guided MNP. After establishing the SMMC-7721 human HCC xenograft in nude mice, followed by the *in situ* formation of the bio-magnet, the external ac magnetic field was directly adopted for magnetic hyperthermia. The tumor could almost completely be treated after the magnetic hyperthermia without obvious reoccurrence (Fig. 6a and b), showing the high magnetic-hyperthermia performance of the implanted bio-magnet for tumor treatment. Most of the current approaches for magnetic hyperthermia using MNPs still suffer from low-targeting efficiency,[41] and the generated temperature is relatively low, up to 40–42 °C,[52] which is not

 

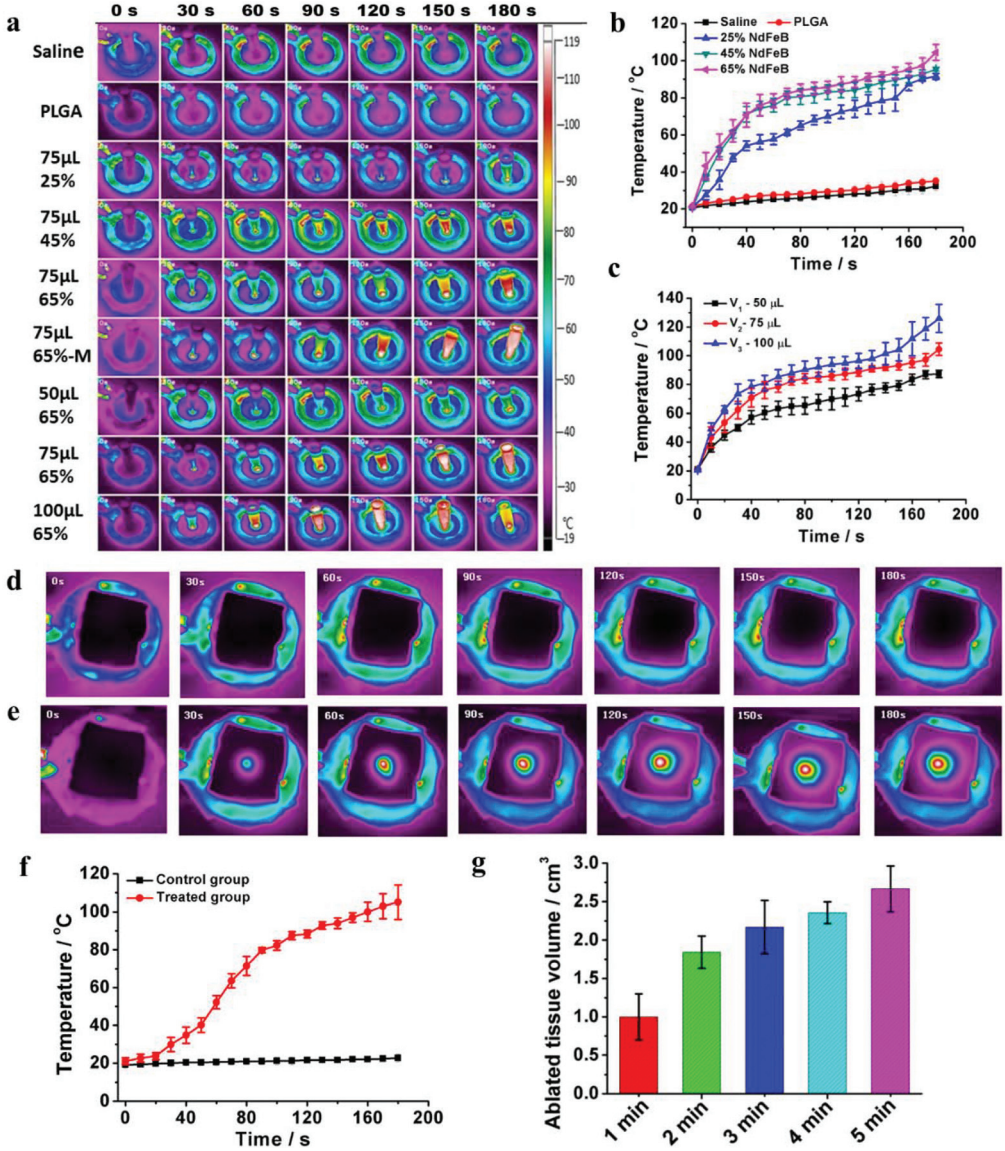


**Fig. 5** Therapeutic performance of the artificial bio-magnet for magnetic hyperthermia. (a) The thermal images of the bio-magnet at different volumes and mass fractions of $Nd_2Fe_{14}B$ after being exposed to ac magnetic field for extended durations (pure PLGA implant as the control group). The corresponding temperature-exposure duration curve at different (b, 75 μL) $Nd_2Fe_{14}B$ content and (c, 65% $Nd_2Fe_{14}B$-bio-magnet) adopted volume. The thermal images of bovine liver after exposure to ac magnetic field (d) without and (e) with implanted 75 μL 65%-bio-magnet for different intervals, and (f) corresponding temperature-exposed duration curves. (g) The ablated tissue volume of bovine liver after being exposed to ac magnetic field for various intervals.

high enough to ablate the tumors. Thus, some researchers are studying the method of using external magnets to concentrate the MNPs, while the external magnet is limited to shallow depth and suffers from the side effects to the skin because of a higher magnetic field in the skin close to the external magnet. The bio-magnet developed in this study was endowed with permanent magnetism within the tumor to highly improve the targeting efficiency, to avoid the side effects to the skin. Moreover, as we know, some tumor receptors might vary after treatment, which affects the targeting efficiency for many targeting therapeutic drugs, while it should not be affected if the bio-magnet is used. In addition, the whole procedure is convenient, which endows the bio-magnet with a strong possibility for future clinical translation.

The implanted bio-magnet possesses high biocompatibility because either the PLGA component or magnetic materials have been extensively demonstrated to be biocompatible.[53,54] In addition, the localized and confined implantation of the bio-magnet is intrinsically featured with high biosafety because the implanted bio-magnet is only present within the tumor rather than other normal tissues/organs. Importantly, the implanted bio-magnet was biodegradable as it was metabolized after the implantation for two months in mice (Fig. 6c–e). The prussian-blue staining results showed that the

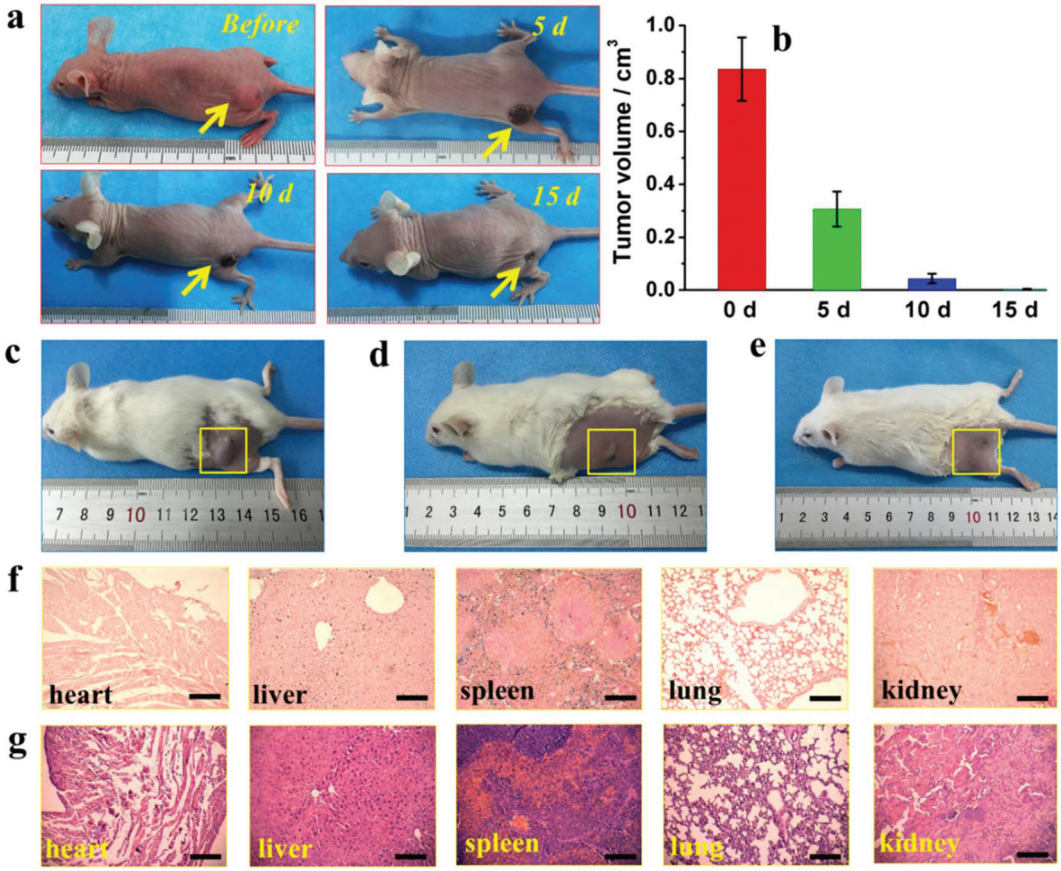


**Fig. 6** *In vivo* magnetic hyperthermia and biocompatibility. (a) Photographs of tumor-bearing mice at different magnetic hyperthermia stages. (b) The tumor volume before and after magnetic hyperthermia for different variations (5 d, 10 d and 15 d). The observation of the degradation process of the bio-magnet in mice after (c) direct implantation and the following feeding for (d) 1 month and (e) 2 months. (f) Prussian-blue staining of the heart, liver, spleen, lung and kidney of mice after 2 months feeding. (g) H&E staining of the hearts, livers, spleens, lungs and kidneys of mice after 2 months feeding (scar bar: 200 μm).

degraded products were found in the liver and spleen of the mice (Fig. 6g). Importantly, the histocompatibility evaluation results based on hematoxylin–eosin (H&E) staining exhibited no obvious pathological changes in the main organs after two months feeding (Fig. 6f), the metabolic mechanism of this artificial bio-magnet will be explored in our next study. Together with the fact that the toxicity of $Nd_2Fe_{14}B$ is low because it has been widely used in basic medical research and clinical applications for a variety of purposes,[42] it is highly expected that the developed implanted bio-magnet possesses high biocompatibility for potential clinical translation.

## Conclusion

In summary, for the first time, we have successfully engineered a new artificial "tumor bio-magnet" for efficiently targeting the circulating MNPs within the blood vessel and achieve simultaneous magnetic hyperthermia. This bio-magnet could be easily implanted by the localized injection of $Nd_2Fe_{14}B/Fe_3O_4$-PLGA, followed by the solvent exchange process for liquid-to-solid transformation. After the magnetization, the solid $Nd_2Fe_{14}B/Fe_3O_4$-PLGA implant exhibited stable magnetic properties and created the intrinsic magnetic field within the tumor tissue, making the tumor an artificial bio-magnet. Intravenously administered MNPs could be effectively attracted and therefore accumulated into the tumor tissue to realize the intrinsic magnetic targeting assisted by the bio-magnet in the tumor. Furthermore, both *in vitro* and *ex vivo* results demonstrated the high efficiency of the implanted bio-magnet for tumor ablation using magnetic hyperthermia. This study presents a new approach for magnetic targeting by creating a unique bio-magnet within the target region. This bio-magnet creates magnetic fields within the target, paving a new way for developing efficient targeting and therapeutic strategies for tumor therapy based on the elaborate design and engineering of the functional biomaterials.

## Ethical statement

All animal procedures were performed in accordance with the Guidelines of the Ministry of Science and Technology of Health Guide for Care and Use of Laboratory Animals, China,

 

and approved by the institutional ethical committee (IEC) of Second Affiliated Hospital of Chongqing Medical University.

## Conflicts of interest

All authors contributed to the written manuscript and have all approved the final version of the manuscript. Bing Liang, Kexiao Yu and Yi Ling are co-first authors who contributed equally to this study. There are no conflicts to declare.

## Acknowledgements

We acknowledge the financial supports from NSF for Distinguished Young Scholars (Grant No. 81425014), National Key R&D Program of China (2018YFC0115200), NSFC Key Projects of International Cooperation and Exchanges (81720108023) and Shanghai S&T Major project (2018SHZDZX05).

## References

1 C. Schmidt, *Nature*, 2015, **527**, S10.
2 A. V. Biankin, S. Piantadosi and S. J. Hollingsworth, *Nature*, 2015, **526**, 361–370.
3 S. Sengupta, D. Eavarone, I. Capila, G. Zhao, N. Watson, T. Kiziltepe and R. Sasisekharan, *Nature*, 2005, **436**, 568–572.
4 V. Wagner, A. Dullaart, A. K. Bock and A. Zweck, *Nat. Biotechnol.*, 2006, **24**, 1211–1217.
5 R. A. Lake and B. W. Robinson, *Nat. Rev. Cancer*, 2005, **5**, 397–405.
6 T. G. Odle, *Radiol. Technol.*, 2014, **85**, 297M.
7 C. Willyard, *Nature*, 2016, **532**, 166–168.
8 R. K. Jain and T. Stylianopoulos, *Nat. Rev. Clin. Oncol.*, 2010, **7**, 653–664.
9 Y. Chen, H. Chen and J. Shi, *Adv. Mater.*, 2013, **25**, 3144–3176.
10 J. T. Jørgensen, *Oncology*, 2013, **85**, 59–68.
11 H. B. Na, I. C. Song and T. Hyeon, *Adv. Mater.*, 2010, **21**, 2133–2148.
12 K. Riehemann, S. W. Schneider, T. A. Luger, B. Godin, M. Ferrari and H. Fuchs, *Angew. Chem., Int. Ed.*, 2009, **48**, 872–897.
13 L. Riccardo and L. Crocetti, *Radiology*, 2012, **262**, 43–58.
14 P. Dan, J. M. Karp, S. Hong, O. C. Farokhzad, R. Margalit and R. Langer, *Nat. Nanotechnol.*, 2007, **2**, 751.
15 G. Szakács, J. K. Paterson, J. A. Ludwig, C. Boothgenthe and M. M. Gottesman, *Nat. Rev. Drug Discovery*, 2006, **5**, 219–234.
16 A. Gabizon, H. Shmeeda, A. T. Horowitz and S. Zalipsky, *Adv. Drug Delivery Rev.*, 2004, **56**, 1177–1192.
17 H. R. Ju, H. Koo, I. C. Sun, S. H. Yuk, K. Choi, K. Kim and I. C. Kwon, *Adv. Drug Delivery Rev.*, 2012, **64**, 1447–1458.
18 X. Gao, Y. Cui, R. M. Levenson, L. W. Chung and S. Nie, *Nat. Biotechnol.*, 2004, **22**, 969–976.
19 Y. Chen, C. Tan, H. Zhang and L. Wang, *Chem. Soc. Rev.*, 2015, **44**, 2681–2701.
20 Y. Chen and J. Shi, *Sci. China Mater.*, 2015, **58**, 241–257.
21 Y. Chen, H. Chen and J. Shi, *Adv. Healthcare Mater.*, 2015, **4**, 158.
22 Y. Chen, L. Wang and J. Shi, *Nano Today*, 2016, **11**, 292–308.
23 H. Koo, M. S. Huh, I. C. Sun, S. H. Yuk, K. Choi, K. Kim and I. C. Kwon, *Acc. Chem. Res.*, 2011, **44**, 1018.
24 E. A. Sykes, Q. Dai, C. D. Sarsons, J. Chen, J. V. Rocheleau, D. M. Hwang, G. Zheng, D. T. Cramb, K. D. Rinker and W. C. Chan, *Proc. Natl. Acad. Sci. U. S. A.*, 2016, **113**, E1142.
25 Y. Chen, L. Jiang, R. Wang, M. Lu, Q. Zhang, Y. Zhou, Z. Wang, G. Lu, P. Liang and H. Ran, *Adv. Mater.*, 2014, **26**, 7468.
26 X. Mou, Z. Ali, S. Li and N. He, *J. Nanosci. Nanotechnol.*, 2015, **15**, 54.
27 J. H. Lee, J. T. Jang, J. S. Choi, S. H. Moon, S. H. Noh, J. W. Kim, J. G. Kim, I. S. Kim, K. I. Park and J. Cheon, *Nat. Nanotechnol.*, 2011, **6**, 418.
28 J. Gao, X. Chen and Z. Zhao, *Journal*, 2016, 222–228.
29 D. Kilinc, C. L. Dennis and G. U. Lee, *Adv. Mater.*, 2016, **28**, 5672–5680.
30 F. Q. Hu, L. Wei, Z. Zhou, Y. L. Ran, Z. Li and M. Y. Gao, *Adv. Mater.*, 2006, **18**, 2553–2556.
31 S. Laurent, D. Forge, M. Port, A. Roch, C. Robic, E. L. Vander and R. N. Muller, *Chem. Rev.*, 2008, **39**, 2064.
32 X. L. Liu and H. M. Fan, *Curr. Opin. Chem. Eng.*, 2014, **4**, 38–46.
33 M. K. Limatenório, E. A. Pineda, N. M. Ahmad, H. Fessi and A. Elaissari, *Int. J. Pharm.*, 2015, **493**, 313–327.
34 K. Jaeyun, L. J. Eun, L. Jinwoo, Y. Jung Ho, K. Byoung Chan, A. Kwangjin, H. Yosun, S. Chae-Ho, P. Je-Geun and K. Jungbae, *J. Am. Chem. Soc.*, 2006, **128**, 688–689.
35 M. Arruebo, R. Fernández-Pacheco, M. R. Ibarra and J. Santamaría, *Nano Today*, 2007, **2**, 22–32.
36 B. Chertok, B. A. Moffat, A. E. David, F. Yu, C. Bergemann, B. D. Ross and V. C. Yang, *Biomaterials*, 2008, **29**, 487–496.
37 G. Mikhaylov, U. Mikac, A. A. Magaeva, V. I. Itin, E. P. Naiden, I. Psakhye, L. Babes, T. Reinheckel, C. Peters and R. Zeiser, *Nat. Nanotechnol.*, 2011, **6**, 594–602.
38 S. S. Leong, Z. Ahmad and J. Lim, *Soft Matter*, 2015, **11**, 6968–6980.
39 A. López, G. Mestres, M. K. Ott, H. Engqvist, S. J. Ferguson, C. Persson and B. Helgason, *J. Mech. Behav. Biomed. Mater.*, 2014, **32**, 245–256.
40 S. A. Stanley, J. E. Gagner, S. Damanpour, M. Yoshida, J. S. Dordick and J. M. Friedman, *Commun. Integr. Biol.*, 2012, **336**, 604–608.
41 S. Manju and K. Sreenivasan, *Langmuir*, 2011, **27**, 14489.
42 C. Hu, C. Tercero, S. Ikeda, M. Nakajima, H. Tajima, Y. Shen, T. Fukuda and F. Arai, *J. Biosci. Bioeng.*, 2013, **116**, 126–131.

43 C. Hu, T. Uchida, C. Tercero, S. Ikeda, K. Ooe, T. Fukuda, F. Arai, M. Negoro and G. Kwon, *J. Biotechnol.*, 2012, **159**, 90–98.
44 C. Yu, J. Ling, W. Ronghui, L. Ming, Z. Qunxia, Z. Yang, W. Zhigang, L. Guangming, L. Ping and R. Haitao, *Adv. Mater.*, 2015, **26**, 7468–7473.
45 M. Blanca San, G. Chafik, E. Martin, R. E. Jung, R. A. Zwahlen, H. Peter, H. G. Schmoekel and F. E. Weber, *Tissue Eng., Part A*, 2009, **15**, 2955.
46 Z. Huang, Y. Shen, N. Pei, A. Sun, J. Xu, Y. Song, G. Huang, X. Sun, S. Zhang and Q. Qin, *Biomaterials*, 2013, **34**, 9905–9916.
47 M. Hoop, F. Mushtaq, C. Hurter, X. Z. Chen, B. J. Nelson and S. Pané, *Nanoscale*, 2016, **8**, 12723.
48 S. Gil, C. R. Correia and J. F. Mano, *Adv. Healthcare Mater.*, 2015, **4**, 883–891.
49 M. Karimi, A. Ghasemi, Z. P. Sahandi, R. Rahighi, S. M. Moosavi Basri, H. Mirshekari, M. Amiri, P. Z. Shafaei, A. Aslani and M. Bozorgomid, *Chem. Soc. Rev.*, 2016, **45**, 1457–1501.
50 L. Joseph R., Quenching of Fluorescence, in *Principles of Fluorescence Spectroscopy*, Springer, Boston, MA, 2006, pp. 277–330, DOI: 10.1007/978-0-387-46312-4_8.
51 N. Ohta and T. Takemura, *J. Chem. Phys.*, 1989, **91**, 4477–4484.
52 M. Mohamed, G. Borchard and O. Jordan, *J. Drug Delivery Sci. Technol.*, 2012, **22**, 393–408.
53 A. Hoornaert, C. D'Arros, M. F. Heymann and P. Layrolle, *Biomed. Mater.*, 2018, **11**, 045012.
54 J. H. Lee, Y. M. Huh, Y. W. Jun, J. W. Seo, J. T. Jang, H. T. Song, S. Kim, E. J. Cho, H. G. Yoon and J. S. Suh, *Nat. Med.*, 2007, **13**, 95–99.